Molecular Therapy
Nucleic Acids
Original Article

Improved cardiac-specific delivery of RAGE siRNA within small extracellular vesicles engineered to express intense cardiac targeting peptide attenuates myocarditis

Hyoeun Kim,[1,2] Dasom Mun,[1,2] Ji-Young Kang,[1] Seung-Hyun Lee,[3] Nuri Yun,[4,5,6] and Boyoung Joung[1,2,6]

[1]Division of Cardiology, Yonsei University College of Medicine, Seoul 03722, Republic of Korea; [2]Brain Korea 21 PLUS Project for Medical Science, Yonsei University, Seoul 03722, Republic of Korea; [3]Department of Biochemistry and Molecular Biology, Yonsei University College of Medicine, Seoul 03722, Republic of Korea; [4]Institute of Life Science & Biotechnology, Yonsei University, Seoul 03722, Republic of Korea; [5]Department of Systems Biology, Yonsei University College of Life Science and Biotechnology, Seoul 03722, Republic of Korea

Small extracellular vesicles (sEVs) are nanometer-sized membranous vesicles secreted by cells, with important roles in physiological and pathological processes. Recent research has established the application of sEVs as therapeutic vehicles in various conditions, including heart disease. However, the high risk of off-target effects is a major barrier for their introduction into the clinic. This study evaluated the use of modified sEVs expressing high levels of cardiac-targeting peptide (CTP) for therapeutic small interfering RNA (siRNA) delivery in myocarditis, an inflammatory disease of heart. sEVs were extracted from the cell culture medium of HEK293 cells stably expressing CTP-LAMP2b (referred to as C-sEVs). The cardiac targeting ability of C-sEVs with the highest CTP-LAMP2b expression was >2-fold greater than that of normal sEVs (N-sEVs). An siRNA targeting the receptor for advanced glycation end products (RAGE) (siRAGE) was selected as a therapeutic siRNA and loaded into C-sEVs. The efficiency of cardiac-specific siRNA delivery via C-sEVs was >2-fold higher than that via N-sEVs. Furthermore, siRAGE-loaded C-sEVs attenuated inflammation in both cell culture and an *in vivo* model of myocarditis. Taken together, C-sEVs may be a useful drug delivery vehicle for the treatment of heart disease.

INTRODUCTION

Extracellular vesicles (EVs) are heterogeneous nanometer- to micrometer-sized membranous vesicles that originate from the endosome or plasma membrane and are secreted into the extracellular space.[1,2] EVs are classified into three main categories based on their size: (1) exosomes (30–200 nm), (2) microvesicles (100–1,000 nm), and (3) apoptotic bodies (1–10 μm).[3,4] As vesicles with diameters ≤200 nm co-sediment with microvesicles, EVs purified via ultracentrifugation at 100,000 × *g* are not the sole constituent of the exosome fraction.[5] Hence, in this study, vesicles of ≤200 nm secreted into the extracellular environment are collectively referred to as small EVs (sEVs).[6]

Heart disease remains a major public health concern globally.[7] Myocarditis, an inflammatory cardiomyopathy, is one of the leading causes of sudden cardiac death in young adults.[8,9] There are various causes of myocarditis, including viral infections and autoimmune disease.[8,10] Furthermore, COVID-19-related myocarditis has been increasingly reported recently.[11] While myocarditis is often spontaneously resolved, some patients require organ transplantation.[12] Unfortunately, an effective curative treatment has not yet been developed.[13,14] Thus, it is imperative to explore new approaches for myocarditis therapy. sEVs are candidate vehicles for the delivery of molecules, such as DNA, RNA, and proteins, in the treatment of heart disease as well as other conditions.[15,16] However, the accumulation of sEVs in off-target organs, such as the liver, spleen, and lung, limits their therapeutic use.[17–19]

The selective delivery of sEVs to target organs, such as the brain or heart, requires genetic modification.[20–22] Recently, cells were manipulated to express LAMP2b, an sEV membrane protein, fused to neuron-specific rabies virus glycoprotein in order to generate sEVs that specifically targeted the brain.[23] Several other studies have also reported the successful local delivery of cardiac-specific EVs.[19,24] We previously enhanced cardiac targeting ability by 15%, using modified exosomes expressing cardiac-targeting peptide (CTP, APWHLSSQYSRT), which specifically targets the heart.[25] However, greater targeting efficiency is required for drug delivery.

Receptor for advanced glycation end products (RAGE) contributes to inflammatory/synaptic processes in heart disease.[26] Furthermore, pharmacological and genetic inhibition of RAGE were both shown to relieve myocarditis.[27] In this study, we evaluated the therapeutic potential of

Received 2 January 2021; accepted 28 April 2021;
https://doi.org/10.1016/j.omtn.2021.04.018.

[6]These authors contributed equally

Correspondence: Boyoung Joung, MD, PhD, Division of Cardiology, Yonsei University College of Medicine, Seoul 03722, Republic of Korea.
E-mail: cby6908@yuhs.ac
Correspondence: Nuri Yun, PhD, Institute of Life Science & Biotechnology, Yonsei University, Seoul 03722, Republic of Korea.
E-mail: yunnuri@hanmail.net

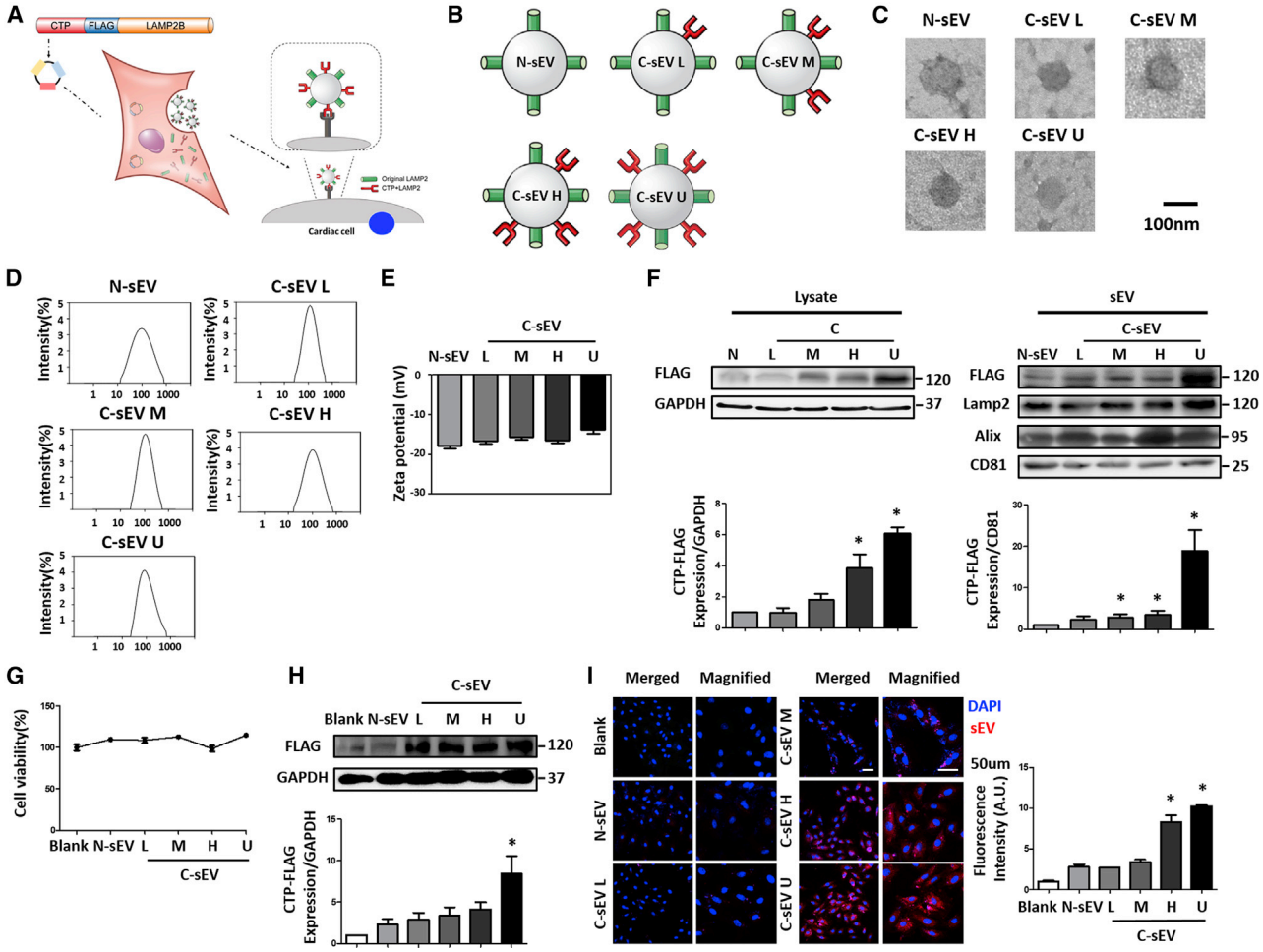

Figure 1. Characterization and cardiac-specific cellular uptake of C-sEVs without cytotoxicity *in vitro*

(A) Schematic representation of sEVs targeting cardiac cells. (B) Schematic representation of targeting via CTP-expressing sEVs. (C–E) TEM images (scale bar, 100 nm) (C), size distribution (D), and zeta potential (E) of sEVs. (F) Western blot analysis of FLAG and GAPDH from stable cell lines as well as FLAG, LAMP2, Alix, and CD81 in sEVs. CTP expression levels were indirectly quantified via the detection of FLAG expression. (G) Cell viability was measured through an MTS assay. (H) Expression of FLAG-LAMP2b in H9C2 cells. (I) Fluorescence microscopy images of PKH26-labeled (red) sEVs in H9C2 cells. Values are expressed as mean ± SEM. *$p < 0.05$ (compared to N-sEVs).

CTP-expressing sEVs (C-sEV) for the delivery of RAGE-targeting small interfering RNA (siRNA) (siRAGE) to suppress myocarditis.

RESULTS

Generation and characterization of C-sEVs

We generated sEVs with high CTP expression for highly efficiently targeting of the cardiac tissue. In particular, we generated several HEK293 cell lines stably expressing CTP-tagged FLAG-LAMP2b and purified sEVs from the culture medium. Based on CTP expression levels, the sEVs were named C-sEV L (low), M (medium), H (high), and U (ultra), respectively. Normal sEVs without CTP expression (N-sEVs) were used as controls (Figure 1B). CTP expression levels were quantified via FLAG-tagged LAMP2b detection. As determined by transmission electron microscopy (TEM), no differences in morphology were observed between N-sEV and C-sEVs (Figure 1C). Additionally, dynamic light scattering (DLS) analysis indicated that C-sEVs and N-sEVs were similar in size (<150 nm) (Figure 1D). To evaluate the stability of sEVs,[28] their zeta potential was measured via electrophoretic light scattering (ELS). A negative zeta potential indicated a high grade of dispersion across sEVs. The zeta potential of isolated sEVs was similar to previously reported values, in the range of −14 to −18 mV (Figure 1E).[29,30] Western blot analysis revealed similar expression patterns of EV markers, such as Alix, CD81, and LAMP2, between N-sEVs and C-sEVs. CTP expression was highest in C-sEV U vesicles and the corresponding cell lysate (Figure 1F). sEVs have been previously described as non-toxic in cells or animals.[31–33] To confirm the safety of sEVs, cell viability was assessed via MTS (3-(4,5-dimethylthiazol-2-yl)-5-(3-carboxymethoxyphenyl)-2-(4-sulfophenyl)-2*H*-tetrazolium) assays in H9C2 rat cardiomyocytes treated with sEVs . There was no significant change in cell viability after treatment with sEVs (Figure 1G). Taken together, CTP expression did not affect the general properties of sEVs.

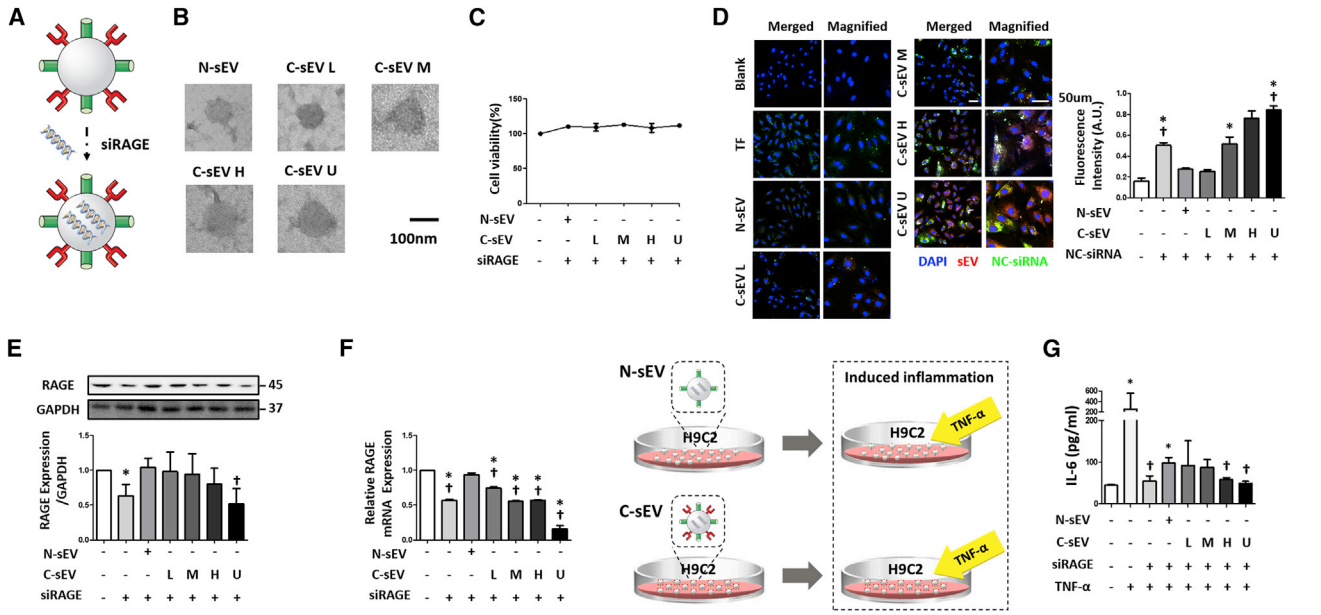

Figure 2. Characterization and effects of siRAGE-loaded C-sEVs in a cellular model of inflammation

(A) Schematic representation of siRNA-loaded sEVs. (B) TEM images of siRAGE-loaded sEVs. H9C2 cells were treated with siRNA-loaded sEVs for 48 h. (C) Measurement of H9C2 cell viability via MTS assays after treatment with siRAGE-loaded sEVs. (D) Fluorescence microscopy images of NC-siRNA-loaded (green) and PKH26-labeled (red) sEVs in H9C2 cells, with cell nuclei (blue). (E) Western blot and (F) qRT-PCR analyses of H9C2 cells treated with siRAGE-loaded sEVs. H9C2 cells were treated with siRAGE-loaded sEVs for 48 h before inducing inflammation via TNF-α treatment for 24 h. (G) Inflammation was monitored through detection of IL-6 levels in culture medium. TF, transfection. Values are expressed as mean ± SEM. *$p < 0.05$ (compared to control); †$p < 0.05$ (compared to N-sEVs). See also Figure S2.

C-sEVs exhibited enhanced cardiac-specific cellular uptake *in vitro*

To determine whether the cardiac cellular uptake of sEVs is dependent on CTP expression levels, we treated H9C2 cells with sEVs and harvested the cells after 24 h. As determined via western blotting, cellular uptake of C-sEV U was significantly greater (i.e., 4-fold higher) than that of N-sEVs (Figure 1H). Fluorescence staining of the lipid membrane is most commonly utilized for monitoring sEV uptake.[34] In this study, PKH26 was used for lipid membrane staining to monitor vesicle uptake by H9C2 cells. Confocal microscopy indicated that the levels of C-sEV H and C-sEV U cellular uptake were 3- and 4-fold higher, respectively, than those observed for N-sEVs (Figure 1I). Thus, we found that sEV cellular uptake into H9C2 cells increased with the sEV CTP expression level.

Characterization of siRNA-loaded sEVs

Bangert et al.[35] reported that knockdown of RAGE protects against inflammatory heart disease. Accordingly, siRAGE was selected to evaluate the therapeutic effect of C-sEV-mediated siRNA delivery in inflammatory heart disease. First, the ratio of siRNA to sEVs was determined in order to establish optimal conditions for maximum association (Figure S1A). As shown in Figure S1A, siRAGE at 600 pmol was loaded into sEVs (40 μg) (Figure 2A). TEM, DLS, ELS, and MTS assays were performed to evaluate the effect of siRAGE loading on sEV properties. sEVs loaded with siRAGE had similar morphology (Figure 2B), size, and zeta potential (Figures S1B and S1C) compared to their non-loaded counterparts. Furthermore, siRAGE-loaded sEVs were non-toxic to cells (Figure 2C). Overall, the general characteristics of sEVs were maintained after siRAGE loading.

C-sEVs loaded with siRNA exhibited enhanced cardiac-specific cellular uptake *in vitro*

To assess whether cardiac-targeted siRNA delivery was enhanced via C-sEVs, PKH26-labeled sEVs (red) were loaded with fluorescence-labeled negative control siRNA (NC-siRNA, green). H9C2 cells were then treated with sEVs loaded with NC-siRNA, and cellular uptake of NC-siRNA was visualized using confocal microscopy after 24 h. We observed the delivery of NC-siRNA to cells via sEVs, with 2- and 3-fold higher uptake efficiency in the C-sEV H and C-sEV U groups, respectively, compared to the N-sEV group (Figure 2D). To evaluate RAGE knockdown efficiency via sEV-mediated siRAGE delivery, H9C2 cells were treated with siRAGE-loaded sEVs for 48 h. Western blot analysis revealed that RAGE silencing was 3-fold more effective in the C-sEV U-treated group than in the N-sEV-treated group (Figure 2E). Quantitative reverse transcription polymerase chain reaction (qRT-PCR) indicated significantly lower RAGE expression in the C-sEV-treated group compared to the N-sEV-treated group. In particular, knockdown efficiency was 6-fold greater in the C-sEV U-treated group than in the N-sEV-treated group (Figure 2F). These results suggested that C-sEVs efficiently deliver siRNAs to cardiomyocytes.

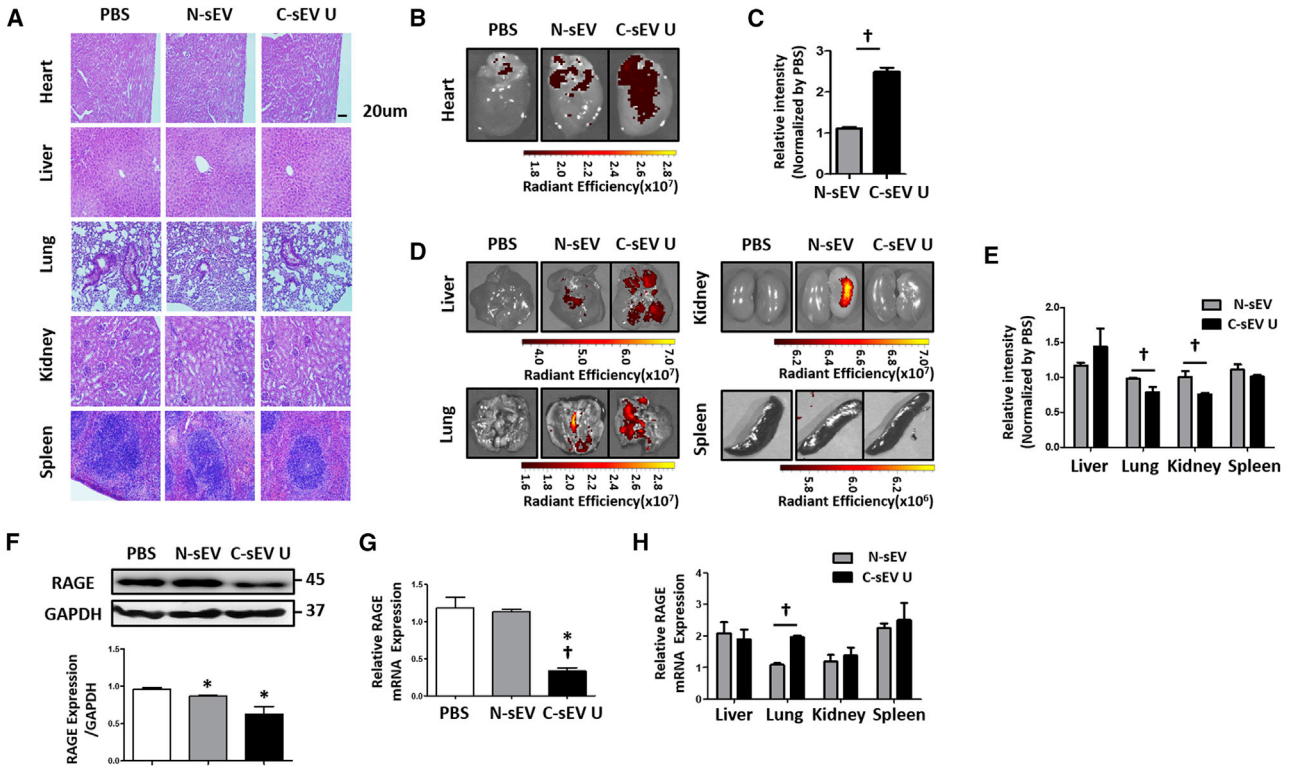

Figure 3. *In vivo* cardiac targeting of C-sEV U without cytotoxicity

(A) H&E staining of the heart, liver, lung, kidney, and spleen 2 days after sEV treatment. (B) Representative near-infrared fluorescence (NIRF) images (overlaid on photograph) of hearts from rats administered PBS or PKH26-labeled sEVs. (C) Quantification of fluorescence intensity in the heart. (D) Representative NIRF images (overlaid on photograph) of rat organs. (E) Quantification of fluorescence intensity in the liver, lung, kidney, and spleen. (F and G) Western blot analysis (F) and qRT-PCR detection (G) of *RAGE* in heart tissue from rats treated with siRAGE-loaded sEVs. (H) qRT-PCR of *RAGE* mRNA in the liver, lung, kidney, and spleen. Values are expressed as the mean ± SEM. *$p < 0.05$ (compared to PBS); †$p < 0.05$ (compared to N-sEVs). See also Figure S3.

siRAGE-loaded C-sEVs suppressed inflammation in an *in vitro* model

A model of tumor necrosis factor (TNF)-α-induced inflammation in H9C2 cells was used to evaluate the effect of siRAGE-loaded sEVs. H9C2 cells were treated with siRAGE-loaded sEVs for 48 h before the induction of inflammation via treatment with TNF-α for 24 h. Enzyme-linked immunosorbent assay (ELISA) results revealed a sharp increase in the levels of interleukin (IL)-6, a pro-inflammatory cytokine, in the TNF-α-treated group. However, IL-6 levels were significantly lower in the C-sEV H/U-treated groups compared to N-sEV-treated group (Figure 2G). Western blot analysis indicated marked decreases in the levels of inflammatory markers, such as RAGE, IL-6, TNF-α, COX2, HMGB1, and phosphorylated (p-)p65/p65, in the C-sEV U-treated group (Figure S2A). Thus, siRAGE delivery via C-sEV U relieves inflammation in TNF-α-treated H9C2 cells.

Cardiac specificity of C-sEVs

After identification of C-sEV U as the most efficient cardiac-targeting carrier *in vitro*, we performed *in vivo* experiments to confirm this. First, we investigated whether siRAGE-loaded sEVs induce systematic toxicity in wild-type Sprague-Dawley (SD) rats. sEVs (100 μg of total protein in sEV precipitate resuspended in 0.5 mL of PBS per rat) or an equal volume of PBS (0.5 mL) were administered via tail vein injection, and rats were sacrificed 24 h later. No pathological changes were observed in any examined organ (Figure 3A). To assess the specific accumulation of siRAGE-loaded sEVs in the heart, we studied the *in vivo* distribution of PKH26-labeled sEVs using an *in vivo* imaging system (IVIS). Fluorescence intensity within the hearts of C-sEV U-injected rats was 200% higher than that observed in N-sEV-injected animals (Figures 3B and 3C). In contrast, with the exception of the liver, fluorescence intensity in other organs (i.e., spleen, lungs, and kidneys) was significantly higher in the N-sEV-injected group (Figures 3D and 3E). These results suggested that C-sEV U accumulates efficiently within the heart and has greater cardiac specificity than N-sEV.

C-sEVs exhibited enhanced cardiomyocyte-specific uptake *in vivo*

To determine the target cell type of C-sEV U in cardiac tissue, immunohistochemistry was performed with cardiomyocyte-specific (cardiac troponin I [cTnI]), cardiac fibroblast-specific (vimentin), and endothelial cell-specific (von Willebrand factor [vWF]) antibodies.

PKH26-labeled C-sEV U co-localized with cTnI, but not with vimentin and vWF (Figure S3). Taken together, these results indicated that C-sEV U is effectively distributed in cardiomyocytes *in vivo*.

Cardiac-specific siRAGE delivery efficiency of C-sEVs *in vivo*

Next, we investigated the *in vivo* RAGE knockdown efficiency via sEV-mediated systemic siRNA delivery. Western blot analysis revealed that RAGE silencing within cardiac tissues was more effective in the siRAGE-loaded C-sEV U-injected group than in the siRAGE-loaded N-sEV-injected group (Figure 3F). Similar results were obtained at the mRNA level via qPCR analysis (Figure 3G). Conversely, with the exception of the liver, *RAGE* mRNA levels in other organs (spleen, lungs, and kidneys) were lower in the siRAGE-loaded N-sEV-injected group than in the siRAGE-loaded C-sEV U-injected group (Figure 3H). These results indicated that the efficiency of siRNA delivery to heart tissue was higher for C-sEV U than for N-sEVs.

C-sEVs loaded with siRAGE suppressed inflammation in experimental autoimmune myocarditis (EAM)

To determine whether the newly developed siRNA delivery tool could be used to treat myocarditis, we administered siRAGE-loaded sEVs in a widely used rat model of EAM. We compared the effects of siRAGE delivery by C-sEV U and N-sEVs. Twenty-one days after initial immunization with cardiac myosin, we performed histological analyses of left ventricular tissues. siRAGE-loaded C-sEV U prevented inflammatory cell infiltration in EAM, and lower inflammation was observed in the siRAGE-loaded C-sEV U-injected group compared to siRAGE-loaded N-sEV-injected group (Figure 4A). Echocardiography revealed better heart function in siRAGE-loaded C-sEV U-injected rats compared to that of their siRAGE-loaded N-sEV-injected counterparts (Figure 4B). Western blot analysis indicated significant reductions in the levels of RAGE, IL-6, TNF-α, COX2, HMGB1, and p-p65/p65 in the former (Figure 4C). Taken together, C-sEV U efficiently delivered therapeutic siRNA to the heart, demonstrating their potential as a drug delivery tool in cardiac disease.

DISCUSSION

In this study, we established four cell lines with different levels of CTP-LAMP2b expression. As the expression level of CTP-LAMP2b increased, so did the cardiac-specific cellular uptake of sEVs (Figure 1). In H9C2 cells, the cardiac targeting efficiency was 4-fold higher for C-sEV U than for N-sEVs (Figure 1). Furthermore, we observed a 2-fold increase in cardiac-specific accumulation for C-sEVs in rats, without toxicity (Figure 3).

Although we have previously demonstrated the efficiency of cardiac-targeting sEVs, the therapeutic effects of siRNA-loaded sEVs have not been evaluated. Thus, we delivered siRAGE to inflammatory H9C2 cells and rats with myocarditis via C-sEVs. siRNA knockdown of RAGE suppressed cardiac inflammation in both models. We also demonstrated that the delivery of siRAGE via C-sEVs relieved inflammation more effectively than through N-sEVs (Figures 2 and 4).

We confirmed that C-sEVs were not toxic and retained sEV characteristics even after siRAGE loading (Figure 2). These results support the clinical introduction of C-sEVs for cardiac-targeted drug delivery. While the current work focused on inflammatory heart diseases, the approach described herein may be applied to a variety of other heart diseases. Furthermore, as sEVs do not trigger an immune response, they are promising candidates for clinical use.[32] Given its capacity for targeted delivery, the vesicle-siRNA system should be further developed, enabling greater therapeutic effects at optimal dosages.

In conclusion, C-sEV U exhibited a 2-fold greater cardiac targeting efficiency relative to N-sEVs. Furthermore, C-sEV U successfully achieved siRNA delivery, relieving inflammation in cell and animal models of inflammatory heart disease. Taken together, the current results highlight the potential of C-sEVs as molecular delivery vehicles in the treatment of heart disease.

MATERIALS AND METHODS

Cloning

pcDNA GNSTM-3-FLAG-10-Lamp2b-HA was a gift from Joshua Leonard (#71293, Addgene, MA, USA). The CTP (APWHLSSQYSRT) nucleotide sequence (5′-GCC CCC TGG CAC CTG TCC TCC CAG TAC TCC CGG ACC-3′) was inserted into this plasmid using a standard PCR method and the following primers: 5′-ACT ATGGGC AGT GGA GCC CCC TGG CAC CTG TCC TCC CAG TAC TCC CGG ACC GAC TAT AAA GAT GAC-3′ and 5′- GTC ATC TTT ATA GTC GGT CCG GGA GTA CTG GGA GGA CAG GTG CCA GGG GGC TCC ACT GCC CAT AGT-3′. The construct was confirmed via DNA sequencing.

Cell culture and sEV isolation

HEK293 cells (Korean Cell Line Bank, Seoul, Korea) and H9C2 cells (ATCC, VA, USA) were maintained in Dulbecco's modified Eagle's medium (DMEM, Welgene, Korea) containing 10% fetal bovine serum (FBS, Young In Frontier, Korea) and 1% penicillin-streptomycin (Gibco, Waltham, MA, USA). Cells were cultured in a humidified incubator at 37°C with 5% CO_2. HEK293 cells were seeded at 1.5×10^6 cells/mL in a 100-mm dish 1 day prior to transfection in order to ensure ~70%–80% confluence on the next day. CTP-tagged FLAG-LAMP2b plasmid (16 μg) was transfected using Lipofectamine 3000 transfection reagent (Thermo Fisher Scientific, Waltham, MA, USA) according to the manufacturer's instructions. Cells stably expressing CTP-tagged FLAG-LAMP2b were selected with hygromycin B and identified via western blotting with an anti-FLAG antibody. Cell lines constitutively expressing the CTP-tagged FLAG-LAMP2b plasmid were seeded at 5×10^6 cells in a 15-cm dish. The cell culture medium was serum-free DMEM supplemented with GlutaMAX (1% final concentration, Gibco). Supernatants were harvested for sEV isolation after 48 h of culture. Cell debris and microvesicles were eliminated from the culture medium via sequential centrifugation, and supernatants were concentrated using a TFF (tangential flow filtration) system with Sartorius 10-kDa (5 L) polyether sulfone membranes.[17] Finally, the sEV fraction was obtained

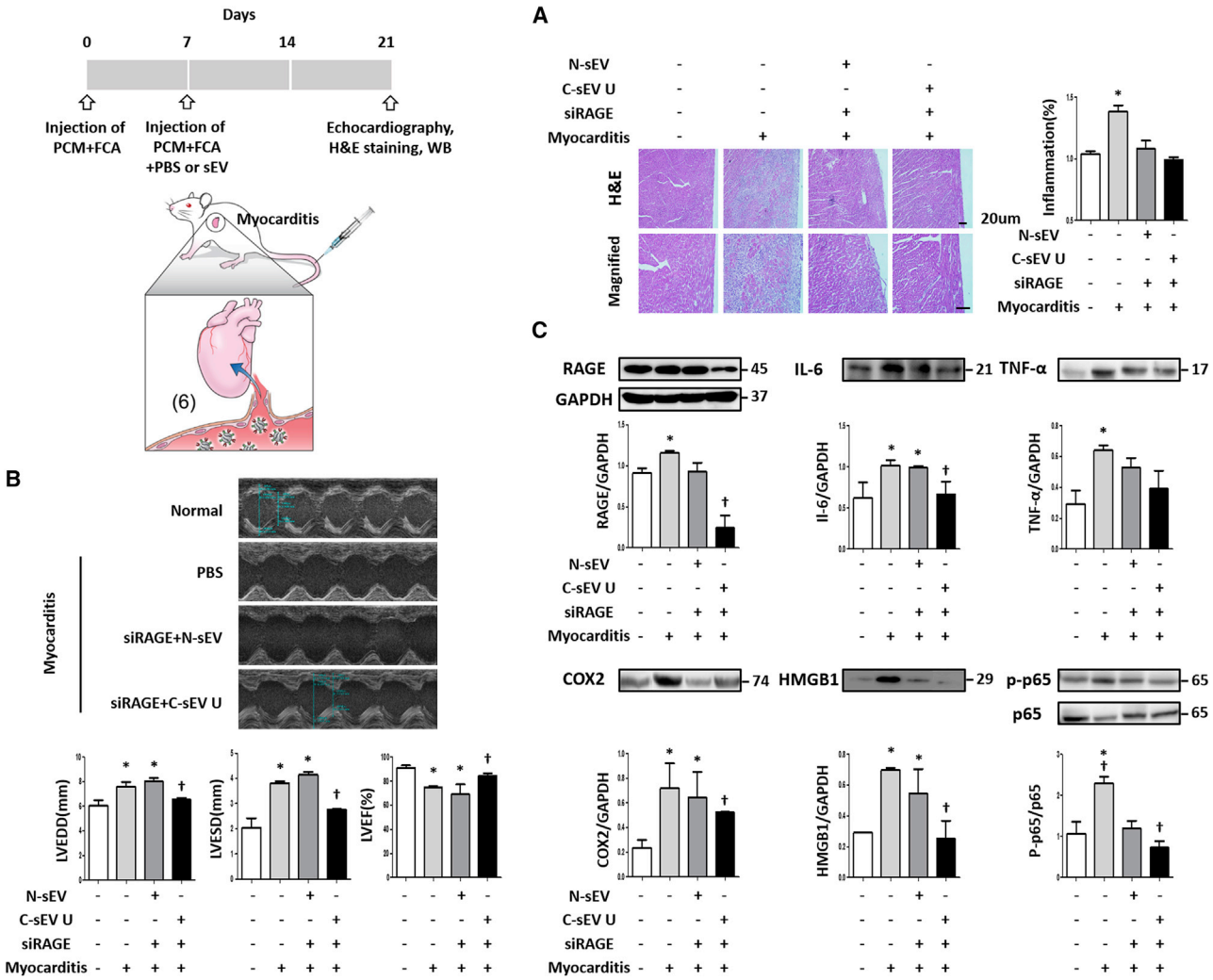

Figure 4. Effects of siRAGE-loaded C-sEV U in a rat EAM model

To induce myocarditis, rats were immunized with purified cardiac myosin derived from porcine ventricular muscle. On days 0 and 7, each rat was subcutaneously injected with an emulsion (0.2 mL) containing cardiac myosin (1.0 mg) in the footpads. On day 7, siRAGE-loaded N-sEVs, C-sEV U, or PBS (control group) was administered. (A) Representative H&E-stained sections of hearts from all four groups. (B) Representative M-mode echocardiograms and comparison of LVEF, LVEDD, and LVESD. (C) Western blot analysis of RAGE, IL-6, TNF- α, COX2, HMGB1, p-p65, p65, and GAPDH. Values are expressed as mean ± SEM. *$p < 0.05$ (compared to normal); †$p < 0.05$ (compared to N-sEVs).

through micro-ultracentrifugation at 100,000 × *g* for 2 h at 4°C (Figure 1A).

Western blot analysis

Western blotting was performed as previously described.[17] Briefly, ultracentrifuged sEV pellets, H9C2 cells, or rat tissues were lysed with radioimmunoprecipitation buffer (ATTO, New York, NY, USA) containing a protease inhibitor cocktail (ATTO). The total protein content was determined via a 660 nm protein assay (Pierce, MA, USA), and equal amounts (20 μg) of sEV, H9C2 cell, or rat tissue protein were separated through sodium dodecyl sulfate-polyacrylamide gel electrophoresis and electrotransferred onto polyvinylidene fluoride membranes. The blots were probed with anti-FLAG (Sigma, Germany), anti-Lamp2 (SC-18822, Santa Cruz Biotechnology, Santa Cruz, CA, USA), anti-CD81 (SC-166029, Santa Cruz Biotechnology), anti-Alix (SC-99010, Santa Cruz Biotechnology), anti-RAGE (ab3611, Abcam, Cambridge, UK), anti-IL-6 (SC-57315, Santa Cruz Biotechnology), anti-COX2 (#4842, Cell Signaling Technology), anti-HMGB1 (#3935, Cell Signaling Technology), anti-p65 (SC-8008, Santa Cruz Biotechnology), p-p65 (SC-136548, Santa Cruz Biotechnology), or anti-TNF-α (#3707, Cell Signaling Technology) at 4°C overnight. The membranes were then probed with horseradish peroxidase-conjugated mouse or rabbit anti-mouse secondary antibodies (Santa Cruz Biotechnology). The protein bands were visualized using chemiluminescence (Advansta, Menlo Park, CA, USA).

Characterization

The DLS machine (DLS7000, Otsuka Electronics, Kyoto, Japan) used in this study had a goniometer with a 35-mW He-Ne laser of 633-nm wavelength. The measurements were performed at a scattering angle of 165°. Light scattering was measured at a controlled temperature of 25.0°C. The values reported in this paper are presented as the average of three replicates. sEVs resuspended in PBS were further diluted with 5 mL of distilled water to determine their size and distribution using an ELS-Z (Otsuka Electronics).

A formvar-carbon-coated electron microscope grid was placed with the formvar side down on top of sEV drops for approximately 1 min. The grid was removed, blotted with filter paper, and placed on a drop of 2% uranyl acetate for 15 s. The excess uranyl acetate was removed, and the electron microscope grid was examined and imaged for TEM. All thin sections were then observed under a TEM (JEM-1011; JEOL, Tokyo, Japan) at an acceleration voltage of 80 kV. Images were captured with a side-mounted Megaview III camera (Soft Imaging System, Münster, Germany).[36]

Immunocytochemistry and confocal microscopy

Immunocytochemistry and confocal microscopy were performed as previously described.[17] After treatment with or without sEVs for 24 h, H9C2 cells were fixed with 4% paraformaldehyde for 60 min at 15–20°C and washed with PBS. Nuclei were stained with 4′,6-diamidino-2-phenylindole (DAPI) (Santa Cruz Biotechnology). Fluorescence microscopy images were obtained under a Zeiss LSM 710 confocal microscope with three excitation filters (405, 488, and 543 nm). Data were recorded as serial optical sections, each consisting of 1,024 × 1,024 pixels, overlaid to distinguish separate emission channels, and saved as TIFF (tagged image file format) files. PKH26, Alexa Fluor 488, and DAPI fluorescence intensities were quantified using the RGB function histogram in ImageJ (National Institutes of Health, Bethesda, MD, USA). Sections were analyzed in triplicate, and the average values were considered.

qRT-PCR analysis

Total RNA was extracted from cultured cells and rat tissues using an RNeasy mini kit (QIAGEN, Hilden, Germany) in accordance with the manufacturer's instructions. cDNA was synthesized using a high-capacity cDNA reverse transcription kit (Applied Biosystems, Foster City, CA, USA) in accordance with the manufacturer's instructions. qRT-PCR was performed using an AriaMx real-time PCR system and Brilliant III Ultra-Fast SYBR Green qPCR master mix (both Agilent Technologies, Santa Clara, CA, USA). The reaction conditions were as follows: 95°C for 3 min, followed by 40 cycles at 95°C for 3 s and 55°C for 20 s. The following PCR primers were synthesized by Cosmo Genetech (Daejeon, Korea): *RAGE* (forward, 5′-GAA TCC TCC CCA ATG GTT CA-3′; reverse, 5′-GCC CGA CAC CGG AAA GT-3′) and *β-actin* (forward, 5′-ATC TGG CAC CAC ACC TTC-3′; reverse, 5′-AGC CAG GTC CAG ACG CA-3′). The relative expression levels of *RAGE* mRNA were calculated via the $2^{-\Delta\Delta CT}$ method[37] and normalized against those of β-actin.

ELISA analysis

IL-6 level in cell culture medium was measured using a fluorometric analysis kit according to the manufacturer's recommendations (Abcam). The samples were analyzed with a plate reader by determining optical density (OD) at a wavelength of 405 nm. Measurements were conducted in triplicate.

Cell proliferation assay and H&E staining

The cytotoxic potential of sEVs was assessed using an MTS assay (Promega, Madison, WI, USA) in accordance with the manufacturer's instructions. H9C2 cells were added to 96-well plates and treated with sEVs in triplicate. Cell survival was determined using an ELISA plate reader (Molecular Devices, Menlo Park, CA, USA). Rat tissues were fixed with 4% formaldehyde, dehydrated with alcohol, embedded in paraffin, chopped into 5-mm slices, and then stained with H&E. Images of ventricular sections from the four groups of rats were made at ×400 magnification (Olympus CX31) and analyzed using ImageJ.

Loading of sEVs with siRNA

The NC-siRNA and siRNA targeting rat RAGE (sense, 5′-CUC UAC GAU CCC AAU UCA A dTdT-3′; antisense, 5′-UUG AAU UGG GAU CGU AGA G dTdG-3′)[38] were obtained from Bioneer (Daejeon, Korea) and transfected into sEVs using Exo-Fect (System Biosciences, Mountain View, CA, USA) in accordance with the manufacturer's instructions. Thereafter, sEVs were incubated with RNase A (Sigma) and washed twice with cold PBS using Amicon ultra centrifugation tubes (EMD Millipore, Billerica, MA, USA). siRNA retention in sEVs was assessed by measuring fluorescence at a maximum excitation emission spectrum of 493–517 nm on a FlexStation 3 fluorescence microplate reader (Molecular Devices). Fluorescence in each sample was compared with the input of FAM-NC-siRNA alone.

Animal Experiments

Male SD rats (weighing 200–250 g each) were purchased from Orient Bio (Seongnam, Korea). All animal experiments were approved by the Institutional Animal Care and Use Committee of Yonsei University College of Medicine (YUMC-2019-0256) and were conducted in accordance with the National Institutes of Health *Guidelines for the Care and Use of Laboratory Animals*.

We injected 100 μg of PKH26-labeled sEVs per rat (n = 3). After 24 h, the heart, liver, spleen, and kidney of each rat were harvested, and the IVIS Spectrum imaging system (PerkinElmer, Waltham, MA, USA) was used to capture near-infrared fluorescence (NIRF) images. Organs were imaged at an excitation wavelength of 551 nm and fluorescence emission at 567 nm. PKH26-related fluorescence signals were distinguished from autofluorescence signals using Living Image software (PerkinElmer).

EAM was induced in SD rats by immunization with porcine cardiac myosin, as previously described.[39] In particular, we administered purified cardiac myosin (M0531, Sigma) from porcine ventricular muscle. Purified cardiac myosin was emulsified with an equal volume of Freund's complete adjuvant (FCA) (F5881, Sigma) containing 1 mg

of *Mycobacterium tuberculosis* (H37Ra, ATCC 25177) at a concentration of 10 mg/mL. On days 0 and 7, rats were subcutaneously injected with 0.2 mL of emulsion in the footpads, for a total of 1.0 mg cardiac myosin per rat. The rats in the normal group received only FCA in the same manner. On day 7, the rats were administered siRAGE-loaded N-sEVs or C-sEV U via tail vein injection. Rats in the normal and PBS groups were treated with equivalent volumes of saline. Three weeks after immunization, echocardiography, H&E staining, and western blot analysis were performed to assess normal, myocarditis, N-sEV-, or C-sEV U-injected rats (each n = 4).

Echocardiography was performed using a Vevo 2100 system (VisualSonics, Toronto, ON, Canada). The left ventricular ejection fraction (LVEF) was calculated according to the following formulas: LVEF (%) = [left ventricular end-diastolic volume (LVEDV) − left ventricular end-systolic volume (LVESV)/LVEDV] × 100; left ventricular fractional shortening (LVFS) (%) = [left ventricular internal-diastolic diameter (LVIDD) − left ventricular internal-systolic diameter (LVISD)/LVIDD] × 100.

Immunohistochemistry

Rat hearts were fixed, dehydrated, frozen, and then sliced into 8 μm-thick cryosections. The sections were incubated with anti-cTnI (1:100; ab47003, Abcam), anti-vWF (1:100; ab6994, Abcam), and anti-vimentin (1:250; ab92547, Abcam) overnight at 4°C in a wet, dark box. Subsequently, sections were incubated with a secondary antibody (Alexa Fluor 488-goat anti-rabbit, 1:500; ab150077, Abcam) for 1 h at room temperature.

Statistical analysis

Data are expressed as the mean ± standard error of the mean (SEM). For multiple comparison analyses, a one-way analysis of variance (ANOVA), followed by a Bonferroni correction, was used. Between-group comparisons were performed via an independent t test. A p value of <0.05 was considered statistically significant. All statistical analyses were conducted using SPSS version 23.0 (SPSS).

SUPPLEMENTAL INFORMATION

Supplemental information can be found online at https://doi.org/10.1016/j.omtn.2021.04.018.

ACKNOWLEDGMENTS

This study was supported by research grants from the Basic Science Research Program through the National Research Foundation of Korea funded by the Ministry of Education, Science and Technology (NRF-2017R1A2B3003303) and from the Korean Healthcare Technology R&D Project funded by the Ministry of Health & Welfare (HI16C0058), as well as by a CMB-Yuhan research grant from Yonsei University College of Medicine for 2019 (6-2019-0124). The authors thank Medical Illustration & Design, part of the Medical Research Support Services of Yonsei University College of Medicine, for all artistic support related to this work.

AUTHOR CONTRIBUTIONS

B.J. and N.Y. conceived and designed the project. B.J. supervised and developed the study. H.K. wrote the manuscript. H.K, D.M., and J.-Y.K. performed the experiments and analyzed the data. S.-H.L. helped to revise the manuscript.

DECLARATION OF INTERESTS

The authors declare no competing interests.

REFERENCES

1. Rayamajhi, S., Nguyen, T.D.T., Marasini, R., and Aryal, S. (2019). Macrophage-derived exosome-mimetic hybrid vesicles for tumor targeted drug delivery. Acta Biomater. *94*, 482–494.
2. Abels, E.R., and Breakefield, X.O. (2016). Introduction to extracellular vesicles: Biogenesis, RNA cargo selection, content, release, and uptake. Cell. Mol. Neurobiol. *36*, 301–312.
3. Maas, S.L.N., Breakefield, X.O., and Weaver, A.M. (2017). Extracellular vesicles: Unique intercellular delivery vehicles. Trends Cell Biol. *27*, 172–188.
4. Takenaka, T., Nakai, S., Katayama, M., Hirano, M., Ueno, N., Noguchi, K., Takatani-Nakase, T., Fujii, I., Kobayashi, S.S., and Nakase, I. (2019). Effects of gefitinib treatment on cellular uptake of extracellular vesicles in EGFR-mutant non-small cell lung cancer cells. Int. J. Pharm. *572*, 118762.
5. Kowal, J., Arras, G., Colombo, M., Jouve, M., Morath, J.P., Primdal-Bengtson, B., Dingli, F., Loew, D., Tkach, M., and Théry, C. (2016). Proteomic comparison defines novel markers to characterize heterogeneous populations of extracellular vesicle subtypes. Proc. Natl. Acad. Sci. USA *113*, E968–E977.
6. Ageta, H., and Tsuchida, K. (2019). Post-translational modification and protein sorting to small extracellular vesicles including exosomes by ubiquitin and UBLs. Cell. Mol. Life Sci. *76*, 4829–4848.
7. Wasala, N.B., Shin, J.H., and Duan, D. (2011). The evolution of heart gene delivery vectors. J. Gene Med. *13*, 557–565.
8. Biesbroek, P.S., Beek, A.M., Germans, T., Niessen, H.W., and van Rossum, A.C. (2015). Diagnosis of myocarditis: Current state and future perspectives. Int. J. Cardiol. *191*, 211–219.
9. Theleman, K.P., Kuiper, J.J., and Roberts, W.C. (2001). Acute myocarditis (predominately lymphocytic) causing sudden death without heart failure. Am. J. Cardiol. *88*, 1078–1083.
10. Caforio, A.L., Pankuweit, S., Arbustini, E., Basso, C., Gimeno-Blanes, J., Felix, S.B., Fu, M., Helio, T., Heymans, S., Jahns, R., et al. (2013). Current state of knowledge on aetiology, diagnosis, management, and therapy of myocarditis: A position statement of the European Society of Cardiology Working Group on Myocardial and Pericardial Diseases. Eur. Heart J. *34*, 2636–2648, 2648a–2648d.
11. Kim, I.C., Kim, J.Y., Kim, H.A., and Han, S. (2020). COVID-19-related myocarditis in a 21-year-old female patient. Eur. Heart J. *41*, 1859.
12. Błyszczuk, P. (2019). Myocarditis in humans and in experimental animal models. Front. Cardiovasc. Med. *6*, 64.
13. Yang, W.I., Lee, D., Lee, D.L., Hong, S.Y., Lee, S.H., Kang, S.M., Choi, D.H., Jang, Y., Kim, S.H., and Park, S. (2014). Blocking the receptor for advanced glycation end product activation attenuates autoimmune myocarditis. Circ. J. *78*, 1197–1205.
14. Arumugam, S., Thandavarayan, R.A., Veeraveedu, P.T., Ma, M., Giridharan, V.V., Arozal, W., Sari, F.R., Sukumaran, V., Lakshmanan, A., Soetikno, V., et al. (2012). Modulation of endoplasmic reticulum stress and cardiomyocyte apoptosis by mulberry leaf diet in experimental autoimmune myocarditis rats. J. Clin. Biochem. Nutr. *50*, 139–144.
15. Shanmuganathan, M., Vughs, J., Noseda, M., and Emanueli, C. (2018). Exosomes: Basic biology and technological advancements suggesting their potential as ischemic heart disease therapeutics. Front. Physiol. *9*, 1159.
16. Le Bras, A. (2018). Exosome-based therapy to repair the injured heart. Nat. Rev. Cardiol. *15*, 382.

17. Kim, H., Yun, N., Mun, D., Kang, J.Y., Lee, S.H., Park, H., Park, H., and Joung, B. (2018). Cardiac-specific delivery by cardiac tissue-targeting peptide-expressing exosomes. Biochem. Biophys. Res. Commun. *499*, 803–808.

18. Sun, D., Zhuang, X., Xiang, X., Liu, Y., Zhang, S., Liu, C., Barnes, S., Grizzle, W., Miller, D., and Zhang, H.G. (2010). A novel nanoparticle drug delivery system: The anti-inflammatory activity of curcumin is enhanced when encapsulated in exosomes. Mol. Ther. *18*, 1606–1614.

19. Mentkowski, K.I., and Lang, J.K. (2019). Exosomes engineered to express a cardiomyocyte binding peptide demonstrate improved cardiac retention in vivo. Sci. Rep. *9*, 10041.

20. French, K.C., Antonyak, M.A., and Cerione, R.A. (2017). Extracellular vesicle docking at the cellular port: Extracellular vesicle binding and uptake. Semin. Cell Dev. Biol. *67*, 48–55.

21. Khongkow, M., Yata, T., Boonrungsiman, S., Ruktanonchai, U.R., Graham, D., and Namdee, K. (2019). Surface modification of gold nanoparticles with neuron-targeted exosome for enhanced blood-brain barrier penetration. Sci. Rep. *9*, 8278.

22. Murphy, D.E., de Jong, O.G., Brouwer, M., Wood, M.J., Lavieu, G., Schiffelers, R.M., and Vader, P. (2019). Extracellular vesicle-based therapeutics: natural versus engineered targeting and trafficking. Exp. Mol. Med. *51*, 1–12.

23. Alvarez-Erviti, L., Seow, Y., Yin, H., Betts, C., Lakhal, S., and Wood, M.J. (2011). Delivery of siRNA to the mouse brain by systemic injection of targeted exosomes. Nat. Biotechnol. *29*, 341–345.

24. Wang, X., Chen, Y., Zhao, Z., Meng, Q., Yu, Y., Sun, J., Yang, Z., Chen, Y., Li, J., Ma, T., et al. (2018). Engineered exosomes with ischemic myocardium-targeting peptide for targeted therapy in myocardial infarction. J. Am. Heart Assoc. *7*, e008737.

25. Zahid, M., Phillips, B.E., Albers, S.M., Giannoukakis, N., Watkins, S.C., and Robbins, P.D. (2010). Identification of a cardiac specific protein transduction domain by in vivo biopanning using a M13 phage peptide display library in mice. PLoS ONE *5*, e12252.

26. Christaki, E., Lazaridis, N., and Opal, S.M. (2012). Receptor for advanced glycation end products in bacterial infection: Is there a role for immune modulation of receptor for advanced glycation end products in the treatment of sepsis? Curr. Opin. Infect. Dis. *25*, 304–311.

27. Yu, Y., Yu, Y., Liu, M., Yu, P., Liu, G., Liu, Y., Su, Y., Jiang, H., and Chen, R. (2016). Ethyl pyruvate attenuated coxsackievirus B3-induced acute viral myocarditis by suppression of HMGB1/RAGE/NF-KB pathway. Springerplus *5*, 215.

28. Beit-Yannai, E., Tabak, S., and Stamer, W.D. (2018). Physical exosome:exosome interactions. J. Cell. Mol. Med. *22*, 2001–2006.

29. Deregibus, M.C., Figliolini, F., D'Antico, S., Manzini, P.M., Pasquino, C., De Lena, M., Tetta, C., Brizzi, M.F., and Camussi, G. (2016). Charge-based precipitation of extracellular vesicles. Int. J. Mol. Med. *38*, 1359–1366.

30. Chang, M., Chang, Y.J., Chao, P.Y., and Yu, Q. (2018). Exosome purification based on PEG-coated Fe_3O_4 nanoparticles. PLoS ONE *13*, e0199438.

31. Mendt, M., Kamerkar, S., Sugimoto, H., McAndrews, K.M., Wu, C.C., Gagea, M., Yang, S., Blanko, E.V.R., Peng, Q., Ma, X., et al. (2018). Generation and testing of clinical-grade exosomes for pancreatic cancer. JCI Insight *3*, e99263.

32. Zhu, X., Badawi, M., Pomeroy, S., Sutaria, D.S., Xie, Z., Baek, A., Jiang, J., Elgamal, O.A., Mo, X., Perle, K., et al. (2017). Comprehensive toxicity and immunogenicity studies reveal minimal effects in mice following sustained dosing of extracellular vesicles derived from HEK293T cells. J. Extracell. Vesicles *6*, 1324730.

33. Maji, S., Yan, I.K., Parasramka, M., Mohankumar, S., Matsuda, A., and Patel, T. (2017). In vitro toxicology studies of extracellular vesicles. J. Appl. Toxicol. *37*, 310–318.

34. Takov, K., Yellon, D.M., and Davidson, S.M. (2017). Confounding factors in vesicle uptake studies using fluorescent lipophilic membrane dyes. J. Extracell. Vesicles *6*, 1388731.

35. Bangert, A., Andrassy, M., Müller, A.M., Bockstahler, M., Fischer, A., Volz, C.H., Leib, C., Göser, S., Korkmaz-Icöz, S., Zittrich, S., et al. (2016). Critical role of RAGE and HMGB1 in inflammatory heart disease. Proc. Natl. Acad. Sci. USA *113*, E155–E164.

36. Kim, S.Y., Kim, H.J., Kim, H.J., Kim, D.H., Han, J.H., Byeon, H.K., Lee, K., and Kim, C.H. (2018). HSPA5 negatively regulates lysosomal activity through ubiquitination of MUL1 in head and neck cancer. Autophagy *14*, 385–403.

37. Livak, K.J., and Schmittgen, T.D. (2001). Analysis of relative gene expression data using real-time quantitative PCR and the $2^{-\Delta\Delta C(T)}$ method. Methods *25*, 402–408.

38. Yang, M.J., Ku, S.H., Kim, D., Kim, W.J., Mok, H., Kim, S.H., and Kwon, I.C. (2015). Enhanced cytoplasmic delivery of RAGE siRNA using bioreducible polyethylenimine-based nanocarriers for myocardial gene therapy. Macromol. Biosci. *15*, 1755–1763.

39. Kodama, M., Matsumoto, Y., Fujiwara, M., Masani, F., Izumi, T., and Shibata, A. (1990). A novel experimental model of giant cell myocarditis induced in rats by immunization with cardiac myosin fraction. Clin. Immunol. Immunopathol. *57*, 250–262.